

ADAPTIVE GRIDS IN NUMERICAL FLUID DYNAMICS

WERNER HAASE

Dornier GmbH, Friedrichshafen, Federal Republic of Germany

KENT MISEGADES

*Cray Research Inc., Mendota Hts., Minnesota, U.S.A.**

AND

MATHIAS NAAR

*Technische Universität Karlsruhe, Federal Republic of Germany**

SUMMARY

A solution adaptive grid (SAG) method which redistributes the nodal points of a function according to its curvature is presented. A single, user-selected step parameter, P , is available for controlling the maximum step size, allowing the application of the technique to a wide variety of problems. Three test cases are cited: (1) the 1-dimensional inviscid Burgers equation, (2) the Falkner–Skan equation and (3) the finite-volume form of the Navier–Stokes equations for transonic aerofoil flows. In all three cases, significant solution improvement in terms of accuracy and convergence acceleration were achieved.

KEY WORDS Solution Adaptive Grids (SAG) Mesh Generation Techniques Burgers Equation Falkner–Skan Equation Viscous Aerofoil Flows Navier–Stokes Equations

INTRODUCTION

Solution adaptive grid (SAG) methods have seen increasing application in recent years. In most cases, the spatial locations of nodal (1-dimension) or mesh (2-dimensions) points are modified during program iteration according to a measure of solution function gradient, curvature or a combination of gradient and curvature. In a fairly early paper that served as a basis for the work described here, Elsholz and Haase¹ used the curvature of wall-normal production density for chemical reactions in boundary layers in order to redistribute nodal points. Dwyer *et al.*² have used a combination of function curvature and gradient in problems concerning fluid dynamics, heat transfer and flame propagation.

Gradients of velocity, internal energy, or Mach number were used in the 2-dimensional mesh adaptation of Gnoffo³ for the supersonic flow about re-entry vehicles. In contrast, Acharya and Patankar⁴ chose the curvature of the temperature distribution for nodal point adaptation in thermodynamics problems. As an exception to these methods, the work of Kutler and Pierson⁵ was aimed at minimizing a measure of numerical truncation error through point redistribution. In all cases, redistribution was carried out at varying frequencies during the iterations, and improvement in solution resolution was clearly evident. Seldom mentioned, however, was the effect of grid adaptation on solution convergence and accuracy.

This paper describes the theory and new applications of the present method. The examples

*Present Address

cited are meant to show the results of only a single adaptation; that is a converged solution to the respective fluid dynamic problem is used as a basis for a supplementary calculation with a new mesh. The advantage of the method described here is its simplicity and applicability to a wide range of problems. The effect of grid adaptation on accuracy and convergence has also been investigated and the results are reported here.

FORMULATION OF THE PROBLEM

In numerical fluid dynamics the equations governing fluid motion are often approximated by the means of difference equations, solved at discrete locations in the finite problem space. Associated with these approximations is a certain amount of numerical error (e.g. truncation error) which we desire to keep as small as possible.

As an example of this, we consider a simple one-dimensional boundary value problem. Using non-uniform spacing, the first derivative may be approximated up to the order $O(h_1, h_2)$ which is $O(h^2)$ if $h_1 = h_2$ or $O(\max(h_1, h_2))$ if $h_1 \neq h_2$ (h_1, h_2 are neighbouring step sizes). The discrete approximation U'_i of a function u'_i can be written as

$$U'_i = u'_i + \frac{1}{6}h_1h_2u'''_i, \quad (1)$$

resulting in a primary local truncation error proportional to the third derivative of u . In general, if the higher order derivatives associated with truncation errors are negligible, then the error itself is negligible. When this is not the case, then the step sizes (h_i) between adjacent points must be decreased.

If constant step sizes are used, this means an increase in the number of grid points over the entire space, which for most problems becomes prohibitively expensive. A logical distribution would place more points in regions where large values of higher order derivatives occur, and fewer points in regions where these derivatives are of minimal significance.

The problem is that we seldom know in advance where exactly large values of these derivatives occur. If however, the computational grid is adapted to preliminary results in such a way as to minimize the aforementioned error term, we can expect the final solution to be an improvement in terms of accuracy over the solutions obtained on uniform or arbitrary grids. In addition, one would expect the same accuracy for this, a so-called 'solution adaptive grid' as for a uniform grid having many more points.

It is assumed that the redistribution of grid points should be based upon the distribution of curvature of the function u shown in Figure 1. The curvature is obtained at each point i by the central difference approximation

$$a_i = u''_i = \frac{2}{h_3} \left\{ \frac{\Delta u_i}{h_2} - \frac{\nabla u_i}{h_1} \right\} + O(h^2, h_2 - h_1), \quad \text{for } i = 2, 3, \dots, N-1, \quad (2)$$

using forward and backward difference operators $\Delta u_i = u_{i+1} - u_i$ and $\nabla u_i = u_i - u_{i-1}$, respectively. For the sake of simplicity we may set $a_1 = a_2$ and $a_N = a_{N-1}$.

By normalizing the curvature with the constant step size h ,

$$h = \frac{x_N - x_1}{N-1}, \quad (3)$$

we obtain a weighted measure k_i of curvature at each point:

$$k_i = |a_i| \frac{h_i}{h}, \quad i = 2, 3, \dots, N, \quad (4)$$

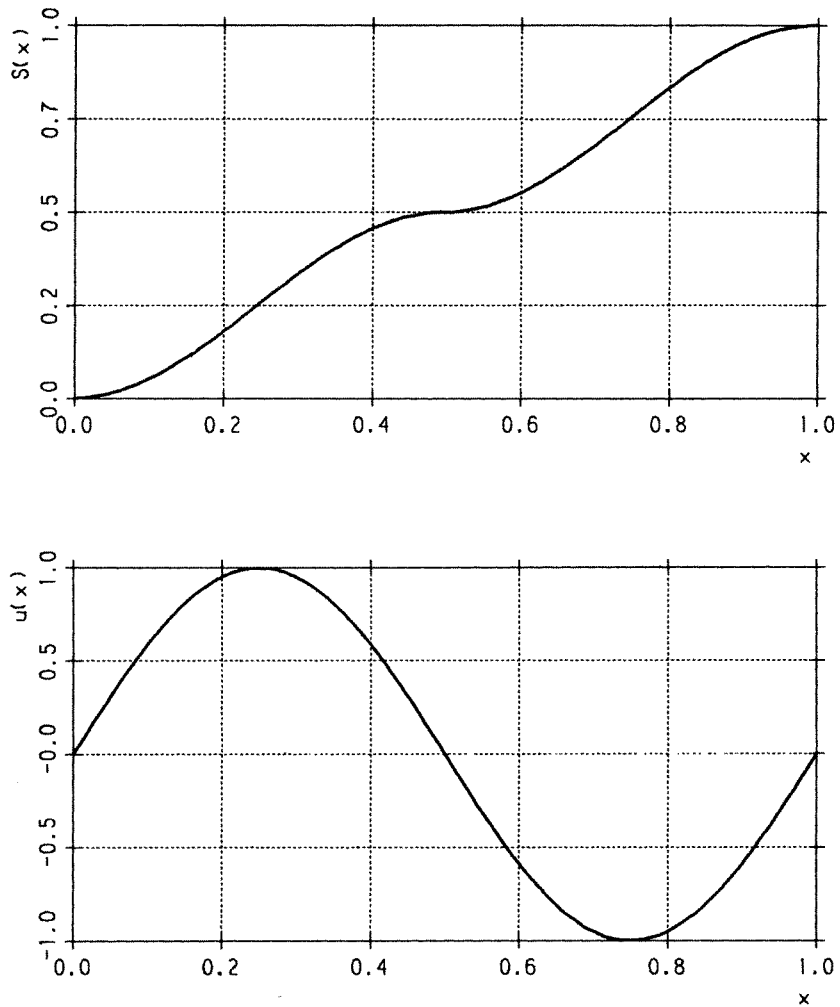


Figure 1. Distribution of a function $u(x)$ and the appropriate transformation function $S(x)$ normalized to unity

with

$$h_i = x_i - x_{i-1}.$$

In order to damp extreme values in curvature and to increase the interval of influence, a new measure of curvature,

$$\alpha_i = \frac{1}{2n+1} \sum_{j=0}^{2n} k_{i+j-n}, \quad i = n+1, \dots, N-n, \tag{5}$$

is introduced for inner points. At boundaries a similar but one-sided formula is used. In all cases described here a value of $n = 1$ was used, resulting in smoothing by three points.

The transformation function is finally obtained from the integration of α (see Figure 1):

$$S_i = \sum_{j=2}^i \alpha_j, \quad \text{with } S_1 = 0. \tag{6}$$

One notices that the transformation function $S(x_i)$ has its maximum slope where the function $u(x_i)$ has its maximum curvature, and its minimum slope where the curvature of $u(x_i)$ is also minimal.

The table of values obtained from $S_i = S(x_i)$ can also be used in its inverse form $x_i = x(S_i)$. By dividing the interval

$$S_N = \frac{1}{h} \int_{x_1}^{x_N} \alpha_i dx$$

into $N - 1$ subintervals,

$$S_i^+ = S_N \frac{i-1}{N-1}, \quad i = 2, 3, \dots, N, \quad (7)$$

one can obtain through interpolation the new distribution $\hat{x}_i = \hat{x}(S_i^+)$. In order to guarantee monotonicity this interpolation must be linear; then from the existence theorem the inverse function exists because S_N is continuous.

The new step sizes found by the procedure just described depend completely on the behaviour of the function $u(x_i)$. If this function is piecewise linear, then some of the α_i become zero. This can lead to uncontrollably large step sizes. Since, however, the accuracy of numerical methods always depends on the chosen step size, an additional condition must be introduced, controlling the maximum interval between two adjacent points. The step parameter P is defined as

$$h_{\max} = Ph, \quad (8)$$

where h is again the step size for a uniform point distribution (see equation (3)).

The gradients of $S(x)$ are now compared against a minimum value

$$q = \frac{S_N}{(N-1)h_{\max}} \neq 0, \quad (9)$$

which is controlled by P . Therefore, it proves necessary to use an additional linear transformation in order to ensure such a minimum gradient of value q .

NUMERICAL EXAMPLES

Inviscid Burgers' equation

The inviscid Burgers' equation with backward step initial conditions has been investigated numerically by several authors.⁶⁻⁹ It may be written in conservation form

$$\frac{\partial u}{\partial t} + \frac{1}{2} \frac{\partial (u^2)}{\partial x} = 0 \quad (10)$$

$$u(x, 0) = \begin{cases} 1, & 0 \leq x < 0.5 \\ 0, & x = 0.5 \\ -1, & 0.5 < x \leq 1 \end{cases} \quad (11)$$

With the initial conditions (11) a steady-state solution will be performed. Therefore, a time-dependent adaptation of grid points is not necessary. Equation (10) is solved numerically using an explicit Runge-Kutta (RK) three step method.¹⁰ In contrast to two-level RK schemes, the extra stage can be used either to improve accuracy or to extend the region of stability. All calculations have been carried out using a Courant number of 1.6 (the stability analysis allows a maximum

Courant number of 2.0) and the $[0, 1]$ -interval divided into 31 subintervals, i.e. 32 nodal points. The method is second order accurate in time and space. Following References 9 and 11, a second order Shuman type filter has been used in order to damp out severe oscillations in the final solution.

Furthermore, the steady-state solution is defined as that solution obtained after reaching the maximum norm

$$\|\varepsilon\| = \max_i^n |u_i^{n+1} - u_i^n|, \tag{12}$$

where n denotes the time level or the iteration count. In each case, ε was chosen to be 5×10^{-4} , taking into account single precision accuracy for an IBM 3083.

As can be seen in Figure 2 severe oscillations are not evident, but compared with the exact solution the numerical one is smeared, the degree of smearing depends on the step parameter P . Furthermore it can be seen that an error measure $|u_{\text{exact}} - u_{\text{numerical}}|$ is nearly constant, independent of P .

Figure 3 gives the iteration count with respect to the step parameter P . It is interesting to recognize that an increase in the value ε for the error norm (from 5×10^{-4} to 5×10^{-3}) causes a constant iteration count for all P . The solution based on a step parameter $P = 1.6$ is defined to be optimal with respect to the minimum number of iteration cycles needed to reach the steady state.

It should be assumed for solving the Burgers equation that a further step-size reduction in the jump region ($P > 1.6$) gives even more accurate results, but there still exists a limitation due to the total number of nodal points. See for example the distribution of grid transformation in Figure 4. From this Figure the concentration of nodal points in the jump region can be seen. For $P = 3$, the maximum step size at the right-hand boundary of the $[0.5, 1]$ interval is three times larger than the constant step size resulting in a significant increase in nodal points within the first 10 per cent of the

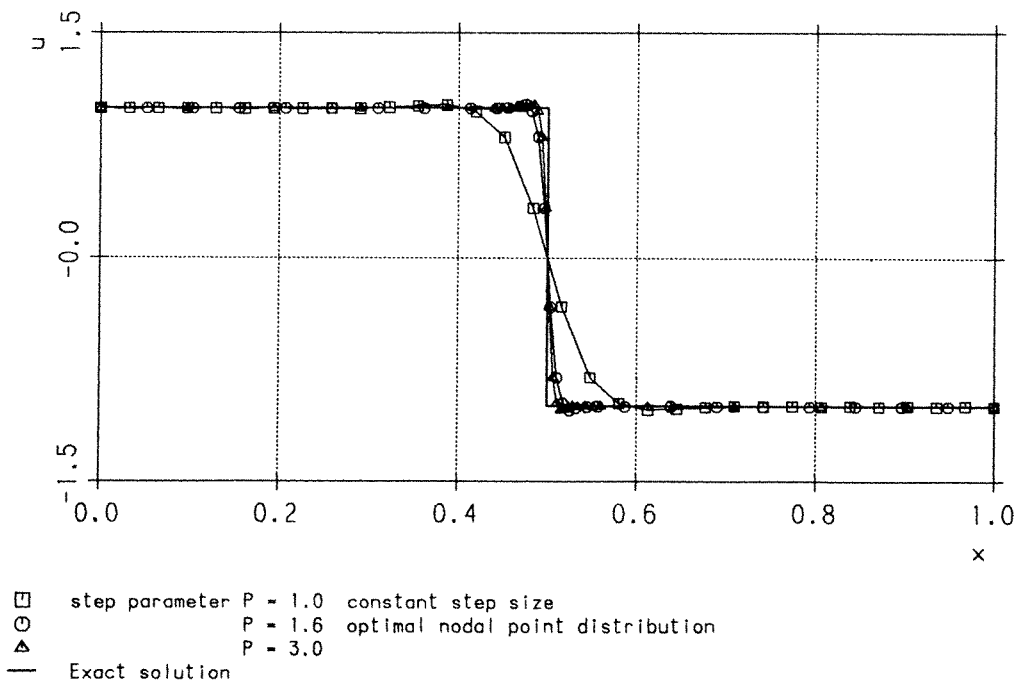
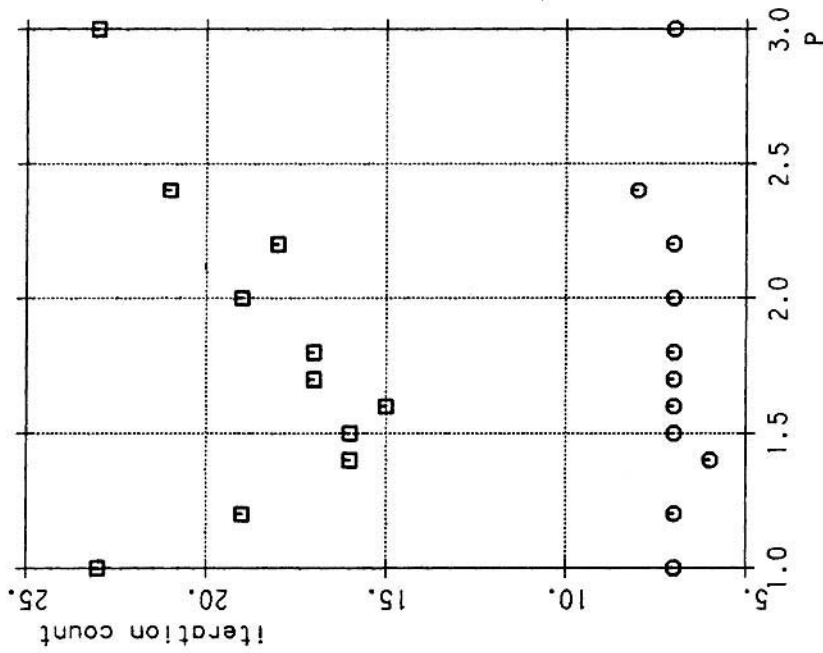


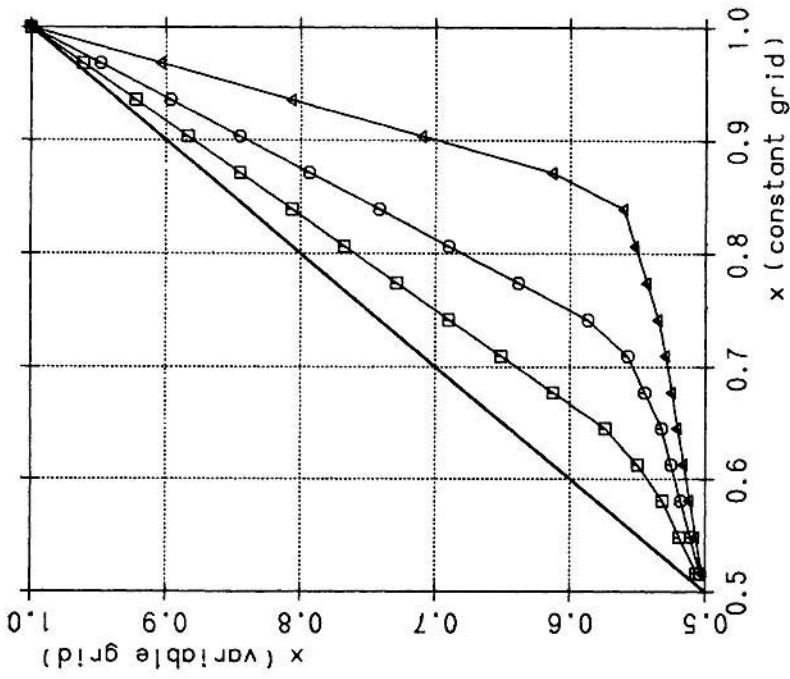





Figure 2. Solution of the inviscid Burgers equation as a function of the step parameter P



 iterative accuracy, maximum-norm $\epsilon = 5 \times 10^{-4}$
 iterative accuracy, maximum-norm $\epsilon = 5 \times 10^{-3}$
 Figure 3. Solution of the inviscid Burgers equation as a function of mesh size—iteration count vs. step parameter P



 step parameter $P = 1.2$
 $P = 1.6$ optimal
 $P = 3.0$
 Figure 4. Solution of the inviscid Burgers equation as a function of mesh size—nodal point distribution as a parameter of P

intervals as well as in a jump in the sequence of mesh points at $x = 0.84$ and a mesh size quotient h_1/h_2 of about 6 at this point. It is obvious that the iteration count will increase, using such large step parameters.

Falkner–Skan boundary layer equation

Laminar, self similar boundary layers in incompressible flows are governed by the Falkner–Skan equation:

$$f''' + ff'' + \beta(1 - f'^2) = 0, \quad (13)$$

with the boundary conditions

$$\begin{aligned} f(0) = f'(0) &= 0, \\ f'(\eta \rightarrow \infty) &= 1. \end{aligned} \quad (14)$$

The prime denotes differentiation with respect to the transformed independent variable η . β is the pressure gradient parameter, being zero for flat plate flow; $\beta = -0.1988$ denotes separation.

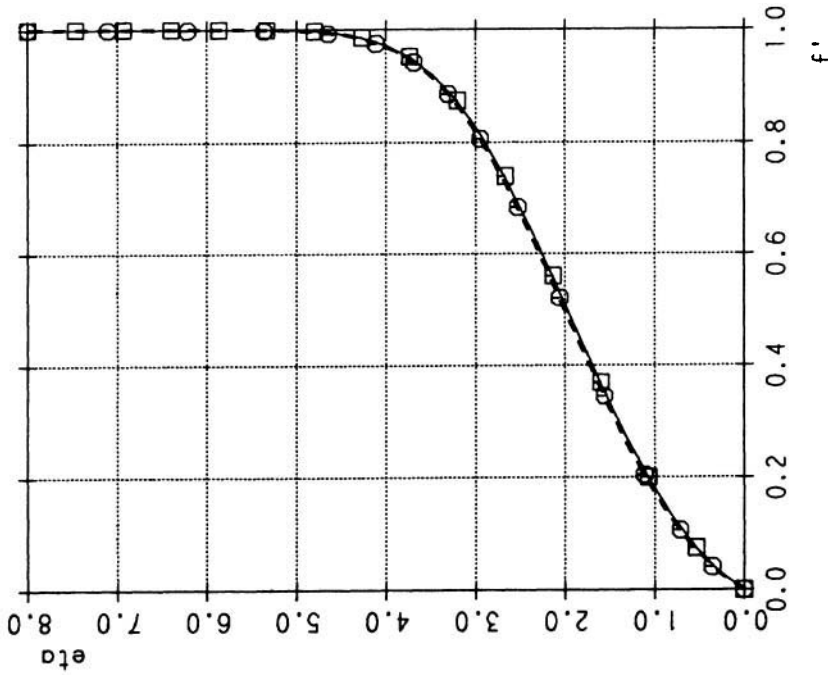
Equation (13) is treated as a non-linear ordinary differential equation in f' . It is solved numerically using an accurate Hermitian difference scheme also known as the Mehrstellen scheme, or collocation method, first proposed by Falk.¹²

The problem is simultaneously solved (1) with N equally spaced grid points, (2) applying the solution adaptive grid technique and (3) with $2N - 1$ points again equally spaced. The calculation shown first uses $\eta_{\max} = 8$, $N = 16$ and $\beta = -0.19$, indicating a boundary layer profile which is close to separation. A converged solution is obtained using the already mentioned error norm (12) of $\varepsilon = 5 \times 10^{-5}$. Comparisons are made with an $N = 181$ solution, defined to be exact. The measure of error is the root-mean-square error between the $N = 181$ and $N = 16$ uniform grid solutions, and the $N = 181$ solution and the interpolated values derived from the unequally spaced $N = 16$ grid, respectively. In Figure 5 the boundary layer profiles resulting from the three different solutions are given, whereas Table I presents the more informative digital output.

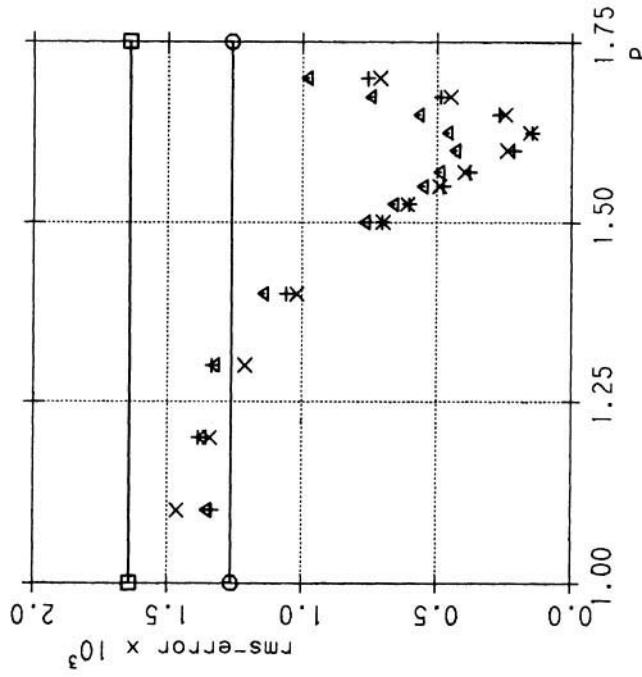
The SAG solution with $P = 1.625$ is defined to be optimal with respect to the root-mean-square error, as shown in Figure 6 given as a function of the interpolation polynomial. The interpolation becomes necessary to calculate the results from the solution adaptive grid approach at appropriate η -stations. Taking into account that the boundary layer profile has only one point of inflection it is evident to use interpolation polynomials of a degree not higher than 3; higher degree polynomials tend to oscillate between the nodal points and, therefore, will not effect the r.m.s. error in a positive way as it can clearly be seen from Figure 6. Included in this Figure are two solid lines denoting the error for the constant grids with $N = 16$ and $2N - 1$ points, respectively. A drastic decrease of the r.m.s. error can be achieved using the present SAG approach instead of doubling the number of nodal points and—roughly—computation time. For the present case and based on the error norm value $\varepsilon = 0.00005$, Table II gives the iterations needed for convergence and the computation time on an IBM 3083.

The appropriate grid transformation function can be taken from Figure 7 for three different step parameters indicating directly the different regions of curvature in the f' distribution. Depending on the gradient of the transformation function one gets an increase in local step sizes where the gradient is larger than unity and vice versa.

For $\beta = 0.0$, which gives the well known Blasius solution, we compared the results of the present methods with those obtained by Reference 5. For $N = 15$, the percentage error measure reduction can be taken from Table III showing clearly the advantage of the present method. I, II, III are



□ constant grid: N=16 points
 ○ variable grid: N=16 points, optimal, P=1.625
 △ constant grid: 2N-1 points
 - - - "exact" solution (based on 181 points)
 Figure 5. Solution of the Falkner-Skan equation with $\beta = -0.19$



□ constant step size using N=16 points
 ○ constant step size using 2N-1 points
 △ variable grid, P=1.625, 1st order interpolation
 × 2nd order interpolation
 * 3rd order interpolation
 Figure 6. Solution of the Falkner-Skan equation with $\beta = -0.19$ —
 rms. error vs. step parameter P

Table I. Solution of the Falkner-Skan equation as a function of mesh size for $\beta = -0.19$

i	η	f'_1	f'_2	f'^3	f'_4
1	0.0	0.0	0.0	0.0	0.0
13	0.53333	0.073829	0.069562	0.072749	0.069346
25	1.06667	0.19981	0.19173	0.19780	0.19115
37	1.60000	0.36945	0.35770	0.36669	0.35743
49	2.13333	0.56085	0.54727	0.55784	0.54742
61	2.66667	0.73981	0.72699	0.73702	0.72748
73	3.20000	0.87364	0.86439	0.87165	0.86459
85	3.73333	0.95120	0.94548	0.95015	0.94585
97	4.26667	0.98521	0.98244	0.98490	0.98258
109	4.80000	0.99645	0.99476	0.99646	0.99521
121	5.33333	0.99929	0.99728	0.99935	0.99860
133	5.86667	0.99987	0.99827	0.99990	0.99941
145	6.40000	0.99997	0.99887	0.99998	0.99965
157	6.93333	0.99999	0.99909	0.99999	0.99979
169	7.46667	1.0	0.99950	1.0	0.99991
181	8.00000	1.0	1.0	1.0	1.0

Subscripts have the following meanings:

- 1: uniform grid: $N = 16$ points
- 2: SAG grid: 2nd order interpolation, $N = 16$ points, optimal ($P = 1.625$)
- 3: uniform grid: $2N - 1$ points
- 4: 'exact' solution based on $N = 181$ points

Table II

$\varepsilon = 0.00005$	Iterations	Computation time (sec)
Uniform grid, $N = 16$	29	0.08
SAG, $N = 16$	33	0.10
Uniform grid, $2N - 1$	37	0.15

Table III Percentage error measure reduction for the Blasius solution

P	k	Present work			Reference 5			
		I	II	III	k	I	II	III
2.15	1	58.16	2.190	1898	1	-14.1	75.2	-118
2.90	7	51.51	2.904	1673	7	76.6	75.2	1.86

k is the order of the interpolation polynomial.

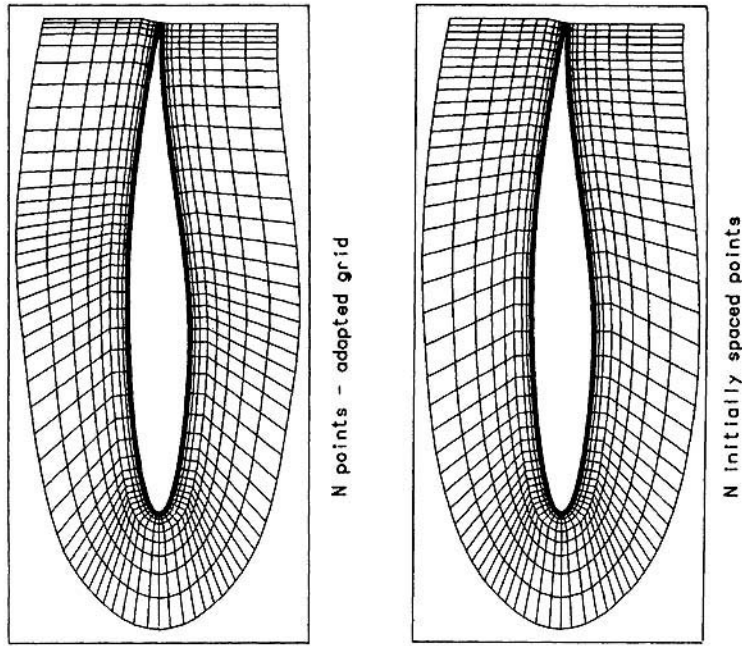
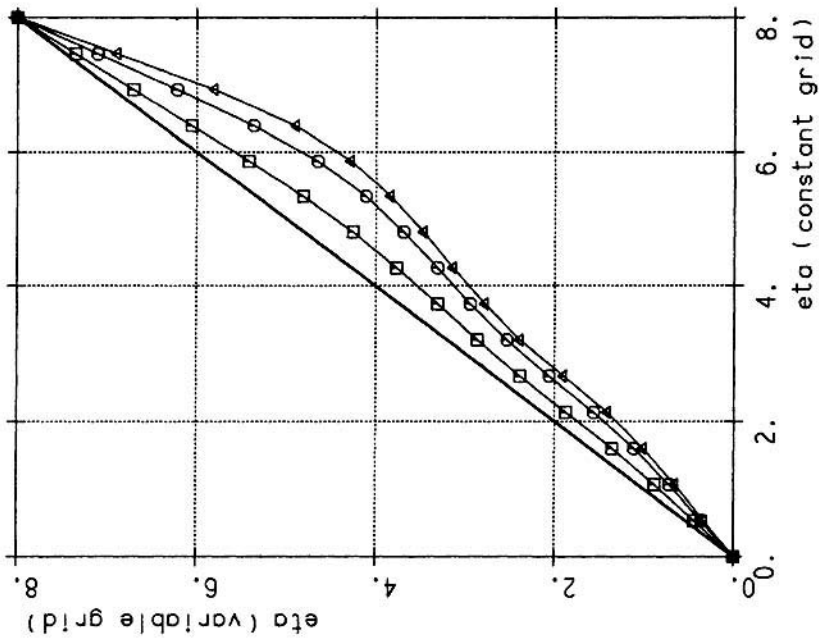


Figure 8. Grid structures for RAE 2822—'case 9' using $N = 83$ points for surface discretization



\square step parameter $P = 1.2$
 \circ $P = 1.625$, optimal
 \triangle $P = 2.0$

Figure 7. Solution of the Falkner-Skan equation with $\beta = -0.19$ —nodal point distribution as a parameter of P

defined to be:

- I: solution using an optimal (SAG) grid compared to that for a uniform grid with N points
- II: solution with $2N - 1$ nodal points compared to that for a uniform grid with N points
- III: improvement between I and II; $\text{III} = (\text{I} - \text{II})/\text{II}$

To conclude at this point of discussion, the presented solution adaptive grid procedure uses the curvature of a given function—not necessarily known in advance—as a transformation function. The results show that this approach leads to an increase in solution accuracy which also means a reduction in truncation error. In Reference 5, however, the third derivative of the function is used as a measure for the transformation, but for schemes with other accuracies—as used here to solve the Falkner–Skan and Navier–Stokes equations—the truncation error is not proportional to the third derivative, but to the fifth for constant step sizes. For this reason, it was not the objective of this work to automatically optimize the truncation error. Instead the step parameter P was included to allow the application of the method to a wide variety of problems, the truncation errors of which are often difficult to estimate accurately. Therefore, one might assume that the present procedure holds for various types of numerical methods and the following discussion associated with two dimensional viscous flow problems is used as a verification.

Viscous flow about the RAE-2822 aerofoil

The presented SAG technique was applied to a two-dimensional flow problem. The compressible, transonic, turbulent flow over the RAE-2822 aerofoil was investigated numerically using a finite volume technique to solve the time-averaged Navier–Stokes equations. In order to simulate a turbulent flow, an algebraic turbulence model¹³ has been used. The finite volume method solves the resulting ordinary differential equations by the means of Runge–Kutta type integration¹⁴ and is closely related to a similar approach for solving the Euler equations, simulating inviscid flows.¹⁰ A body-fitted co-ordinate system permits a reasonable resolution of the rotational layers.

The redistribution of mesh lines emanating from the aerofoil surface is based on the previously calculated pressure coefficient distribution along the surface. This redistribution presented the difficulty that the curvature of the pressure distribution is extremely large at the leading edge, resulting in an undesirably high concentration of points there. This left few points for mesh redistribution in the areas of interest, the shock region and the trailing edge. Thus the SAG method used was modified somewhat, allowing for the exclusion of the leading edge in the redistribution. The junction between the leading edge and the remainder of the aerofoil proved at first to give rise to a large jump in mesh line step sizes. This was corrected with 3 sweeps of a Shuman filter over the newly distributed co-ordinates. An additional modification of the method was the treatment of the curvature of the pressure coefficient distribution at the trailing edge. Here, the values for a_1 (lower surface) and a_N (upper surface) appearing in equation (2) were not set equal to neighbouring values, but were instead calculated as in equation (2) using in both cases the first point in the wake behind the trailing edge. This was necessary in order to take into account the high dissimilarity in the pressure coefficient distribution on the upper and lower surfaces of the trailing edge for the chosen flow problem.

As a demonstration of the effect of applying the SAG technique, the following test case has been performed for the RAE 2822 aerofoil, 'case 9' in Reference 15.

The calculations are based on the uncorrected values: Mach number = 0.73, Reynolds number = 6.5×10^6 , angle of attack = 3.19° .

Eighty-three mesh points were used to represent the aerofoil surface and 32 mesh lines in the

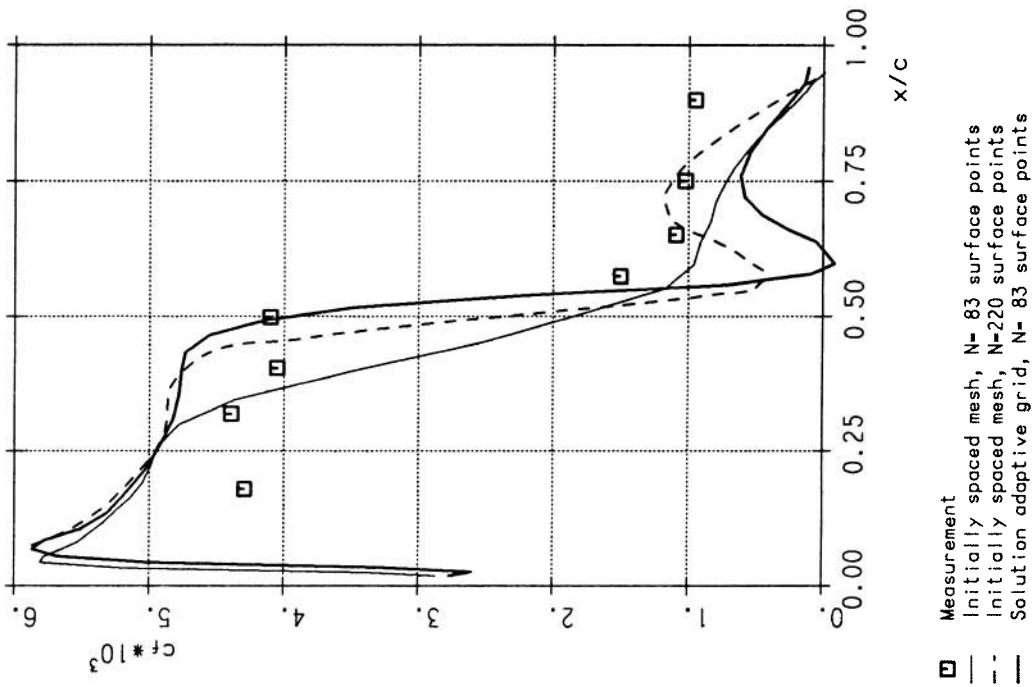


Figure 10. Upper surface skin friction distribution for RAE 2822—'case 9'

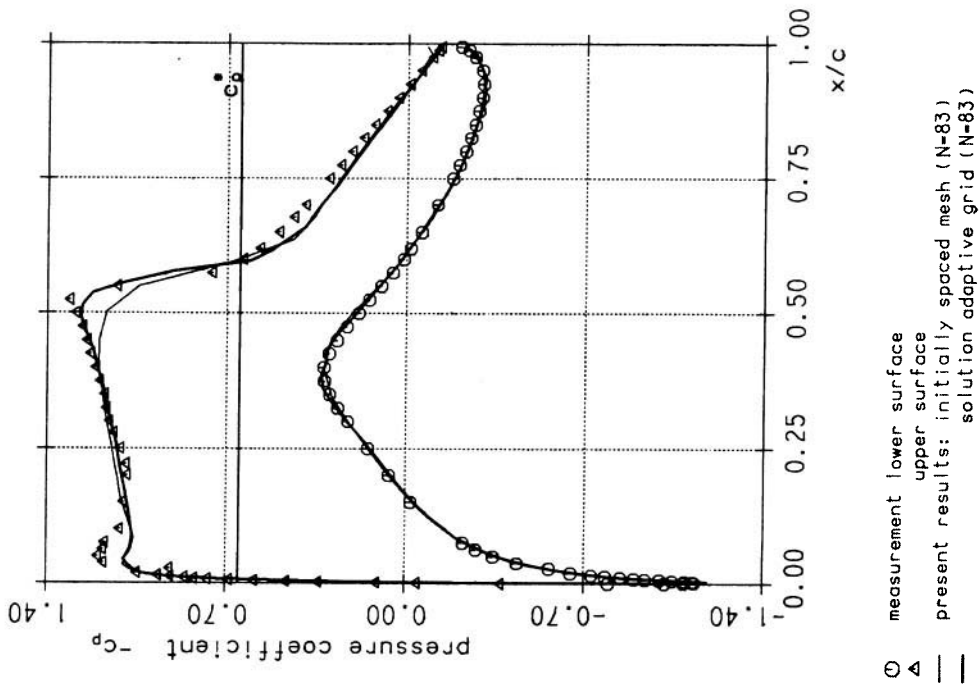


Figure 9. Wall pressure coefficient distribution for RAE 2822—'case 9'

direction moving away from the surface. A total number of 128 mesh lines refers to the number of surface co-ordinates + wake co-ordinates using a C-type mesh.

The initial point spacing, see the lower mesh in Figure 8, is already non-uniform, having more concentrated points at the leading and trailing edges; in these regions a pressure distribution is assumed *a priori* showing larger curvature. The adapted grid in the upper part of the same Figure, is based on the surface pressure distribution calculated by means of the initial mesh. Therefore, concentrations of mesh points at the approximate middle of the upper and lower surface as well as at the trailing edge are due to the curvature of that pressure distribution.

Figure 9 presents the pressure coefficient distribution for the two meshes. The effect of the present solution adaption grid technique can easily be recognized. On the upper surface the shock region is much better represented as well as the pressure plateau in front of the shock. Furthermore, at the lower surface a better correspondence of the calculation with the measurement can be found at the start of the recompression region at about 40 per cent chord length. The poor correspondence of c_p distributions for both meshes at the end of the shock region is thought to be related to boundary layer history effects as well as to shock-boundary-layer interaction problems which cannot be prescribed by the turbulence model used.

Of significance in the prediction of aerofoil force coefficients is the calculation of the wall skin friction coefficient, c_f (see Figure 10). In this Figure the results of the solution adaptive grid technique can be compared with results obtained by initially spaced meshes for $N = 83$ and $N = 220$ surface points as well as with measurements. Furthermore, but already indicated by the pressure distribution, a much better representation of the shock region can be obtained by the SAG approach. For the initially spaced mesh ($N = 83$ surface points) the boundary layer recognizes the pressure distribution on the upper surface as a steep pressure rise only, and not as a shock. The skin friction distribution based on the SAG technique (thick solid line) leads to a slight overprediction of the relaxation of the boundary layer in the region behind the shock as can be seen by comparing it with a solution in a much finer mesh with $N = 220$ surface points.

To conclude at this point, the improvement of the solution accuracy which can be obtained by the present SAG method is appreciable. This can be underlined by comparing the computational efforts in Table IV.

The computational time is based on a comparable convergence behaviour, i.e. for both cases the drag and lift coefficients differ only less than 0.1 per cent per timestep. Assuming the worse case, e.g. using a converged solution in the $N = 83$ mesh, applying the present SAG method (seconds of computer time) and performing a complete new calculation from scratch again, leads only to a doubling of computation time. Therefore, based on the fine mesh results a comparable accuracy can be achieved by use of the present SAG technique with a computing time reduction of 75 per cent.

Table IV. Computational effort

Number of grid points		Computation time (h) IBM 3038
On the surface	Total	
83	4224	1.6
220	18980	13.0

CONCLUSIONS

The conclusions from the work described in this paper are:

- (i) The use of the present SAG technique results in significant improvement with respect to increased accuracy and/or accelerated convergence.
- (ii) The application of the method to the Burgers and Falkner–Skan equations has provided the same or even better results as for calculations with twice the number of grid points evenly distributed.
- (iii) The user specified parameter, P , allows the ‘fine-tuning’ of the method for any particular problem. This is important for the maintenance of overall accuracy as well as for a ‘general purpose’ routine.
- (iv) The method (which exists as a stand-alone routine) can easily be added to existing programs. The technique has proved to be very simple in its application, with negligible increase in computation time.
- (iv) In all examples a redistribution of step sizes was based on converged calculations. The real benefit of such a method, however, comes by redistributing points during a calculation. This can easily be done after each single iteration or after a given number of iterations until convergence is reached.

REFERENCES

1. E. Elsholz and W. Haase, ‘Ein automatisches Verfahren zur Anpassung der Stützstellenverteilung an eine Lösungsfunktion’, *Interner Bericht Nr. 3*, Technische Universität Berlin, Institut für Überschalltechnik, 1972.
2. H. A. Dwyer, R. J. Kee and B. R. Sanders, ‘An adaptive grid method for problems in fluid mechanics and heat transfer’, *AIAA Paper 79-1464*, 1979.
3. P. A. Gnoffo, ‘A vectorized, finite-volume, adaptive grid algorithm applied to planetary entry problems’, *AIAA Paper 82-1018*, June 1982.
4. S. Acharya and S. V. Patankar, ‘Use of an adaptive grid for parabolic flows’, *AIAA Paper 82-1015*, June 1982.
5. P. Kutler and B. L. Pierson, ‘Optimal nodal point distribution for improved accuracy in computational fluid dynamics’, *AIAA Journal*, **18**, (1), 49–53 (1980).
6. E. R. Benton and W. Platzman, ‘A table of solutions of the one-dimensional Burgers equation’, *Quarterly of Applied Mathematics*, 195–212 (1972).
7. R. B. Kellogg, G. R. Shubin and A. B. Stephens, ‘Uniqueness and the cell-Reynolds number’, *SIAM J. Numerical Analysis*, **17**, (6) 733–739 (1980).
8. R. W. MacCormack, ‘Status and future prospects of using numerical methods to study complex flows at high Reynolds numbers’, *AGARD, Lecture Series No. 94*, 1978.
9. M. Naar, ‘Untersuchung zweier moderner Differenzenverfahren und ihre Anwendung auf Probleme der Strömungsmechanik’, *Dornier Bericht Nr. 82 BF/18B*, 1982.
10. W. Haase and M. Naar, ‘Hyperbolic solvers for the Euler equations’, in *Proceeding of Mathematical Methods in Fluid Mechanics*, B. Brosowski and E. Martensen (eds), Peter Lang Publication, 1982.
11. A. Jameson, W. Schmidt and E. Turkel, ‘Numerical solutions of the Euler equations by finite volume methods using Runge–Kutta time stepping schemes’, *Proceedings of AIAA Comp. Flid. Dyn. Conf.*, June 1981.
12. S. Falk, *Zeitschrift für angewandte Mathematik und Mechanik (ZAMM)*, **45** (1965).
13. B. Baldwin and H. Lomax, ‘Thin-layer approximation and algebraic model for separated turbulent flows’, *AIAA Paper 78-257*, 1978.
14. W. Haase, W. Wagner and A. Jameson, ‘Development of a Navier–Stokes method based on finite volume solution techniques for the time-dependent Euler equation’, *Proceedings of the GAMM-Conference on Numerical Methods in Fluid Mechanics*, in *Notes on Numerical Fluid Mechanics*, Vol. 7, Vieweg-Verlag, 1984.
15. P. H. Cook, M. A. McDonald and M. C. P. Firmin, ‘Aerofoil RAE 2822—pressure distributions, and boundary layer and wake measurements’, *AGARD—AR—138*, 1979.